8   Particle Physics with CMS

E. Alagöz, C. Amsler, V. Chiochia, C. Hörmann, K. Prokofiev[5] , H. Pruys[6], C. Regenfus, P. Robmann, J. Rochet, T. Speer, S. Steiner, D. Tsirigkas[7], and L. Wilke

In collaboration with: ETH - Zürich, Paul Scherrer Institut (PSI) and the CMS Collaboration

Physics at the LHC is the main activity of the Zurich group. We are interested in B-physics issues which can be performed during the first 2- 3 years of LHC operation, when the luminosity will still be too low for Higgs searches. In particular, we are preparing with the decay $B_s^0 \to (J/\psi)\phi \to \mu^+\mu^-K^+K^-$ a measurement of $B_s^0 - \bar{B}_s^0$ oscillations, of the lifetime of the CP-eigenstates B_s^H and B_s^L, and of CP-violation. Our group is contributing to the CMS reconstruction and simulation software using the pixel vertex detector required to efficiently tag B-decays. T. Speer has been appointed CMS coordinator for B - tagging. We are involved in the design, construction and test of the barrel pixel detector, a three layer cylindrical silicon device built mostly by Swiss institutions. We are responsible for performance measurements on test beams at CERN (such as position resolution, Lorentz angle and efficiency) on highly irradiated prototypes, and are leading the preparation of the online performance monitoring programs. V. Chiochia is coordinating the CMS pixel offline software group. We are also involved in the development of the sensor readout chip at PSI, and of the power distribution to the pixel detector. The mechanical support structure, cooling system and service tubes are built in the workshop of the Physik-Institut. Details on the software and detector performance can be found in the physics technical design report (1).

8.1   B - physics with CMS

The LHC will be commissioned in 2007 with an initial luminosity of about $10^{30} - 10^{33}$ cm^{-2}s^{-1}. An integrated luminosity of 30 fb^{-1} will be collected after three years of data-taking (assuming an overall beam and detector on efficiency of 30%), after which the luminosity will hopefully reach the design value of 10^{34} cm^{-2}s^{-1}. The main motivation for CMS is the search for the Higgs boson and for supersymmetric particles. However, unless the Higgs is heavy, a significant signal will not be observed during the first 2 - 3 years of operation at low luminosity. Meanwhile, our group intends to concentrate on issues related to the B_s-meson, making full use of the pixel vertex detector.

We intend to perform a high statistics study of the channel $B_s^0 \to (J/\psi)\phi$ with $J/\psi \to \mu^+\mu^-$ and $\phi \to K^+K^-$. This is a good channel to study many properties of B_s^0 - mesons, such as CP - violation, $B_s^0 - \bar{B}_s^0$ oscillations, and to measure the lifetimes of the two eigenstates, B_s^H and B_s^L. The pixel detector is an essential component for these studies requiring a precise determination of the mean life of the B_s^0-meson. Its relatively long lifetime (1.46 ± 0.06 ps) can be used to reject the short-lived background.

B_s^0 - $\bar{B}_s^0$ oscillations have not been observed so far since the oscillation frequency Δm_s is large. The lower limit (95% C.L.) on Δm_s is currently 14.4 ps^{-1} (2). The relative difference between the mean lives of B_s^H and B_s^L is also predicted to be large, in the range 10 - 20%.

CP - violation and particle-antiparticle mixing can also be studied with $B_s^0 \to (J/\psi)\phi$. This

---

[5]until September 2005
[6]until August 2005
[7]CERN doctoral student

decay proceeds mainly through the tree spectator diagram (Fig. 8.1a), second order processes (such as penguin diagrams, Fig. 8.1b) being suppressed.

A full reconstruction of the B_s^0 is achieved through the decays $J/\psi \to \mu^+\mu^-$ and $\phi \to K^+K^-$. CP - violation is induced by interference between the decay and particle–antiparticle mixing. One measures the (CP - violating) asymmetry between $B_s^0 \to (J/\psi)\phi$ and $\bar{B}_s^0 \to (J/\psi)\phi$ which requires tagging the flavor of the B_s^0. An alternative method is to measure the angular distributions of the final state kaons and muons. The CP - even and CP - odd components correspond to even, respectively odd, relative angular momenta between the J/ψ and the ϕ, and have therefore different angular distributions (3). This does not require tagging but very large data samples which can be obtained at the LHC. The decay rate asymmetry determines the CP - violating weak phase $\phi_{CKM} = 2\lambda^2\eta$, where $\lambda \equiv V_{us}$ and η is the height of the unitarity triangle, expected to be very small (about 0.03). The measurement of a significantly larger phase would indicate contributions from processes beyond the standard model.

The branching fraction for $B_s^0 \to (J/\psi)\phi$ is about 10^{-3} (2). With the help of simulations we have developed a selection strategy for the final state $K^+K^-\mu^+\mu^-$ relying on the reconstruction of the four charged particles by a high level trigger (HLT) (4). An event of this type is shown in Fig. 8.2. The muon trigger selects two muons of opposite charges from the muon chambers with a transverse momentum above 3 GeV/c. We require two muons tracks of opposite charges with mass within 100 MeV of the J/ψ mass, and two kaon tracks of opposite charges with mass within 100 MeV of the ϕ mass. The four tracks are required to come from a common secondary vertex. The trigger efficiency is about 10% (4).

Considerable progress was made in 2005 in the development of the tracking and vertex software (5). A general kinematic fitting program was developed for CMS (4). The kinematic fit can be applied to $B_s \to (J/\psi)\phi \to K^+K^-\mu^+\mu^-$ during offline reconstruction to increase the experimental resolution on the B_s^0 mass which improves from 34 MeV to 14 MeV (Fig. 8.3).

Figure 8.1: Feynman diagram for the $B_s^0 \to (J/\psi)\phi$ **decay (a). The penguin diagram (b) is suppressed.**

Figure 8.2: A typical simulated event at CMS which contains a decay of the type $B_s^0 \to (J/\psi)\phi \to \mu^+\mu^-K^+K^-$.

Some 250'000 signal events would be reconstructed after 2 years of LHC running with a background of about 40'000 events. For comparison, only a few hundred events have been
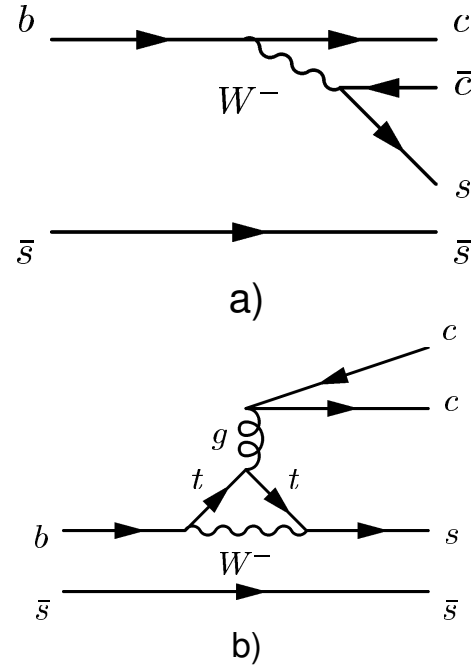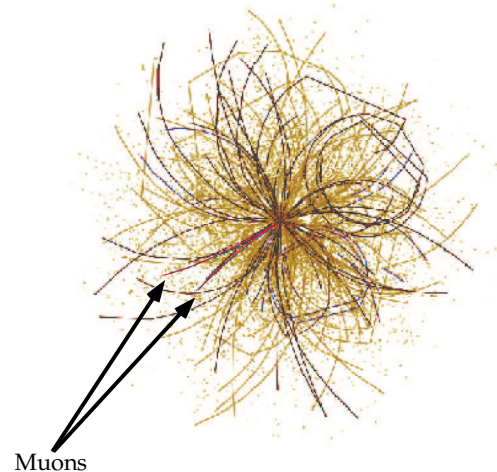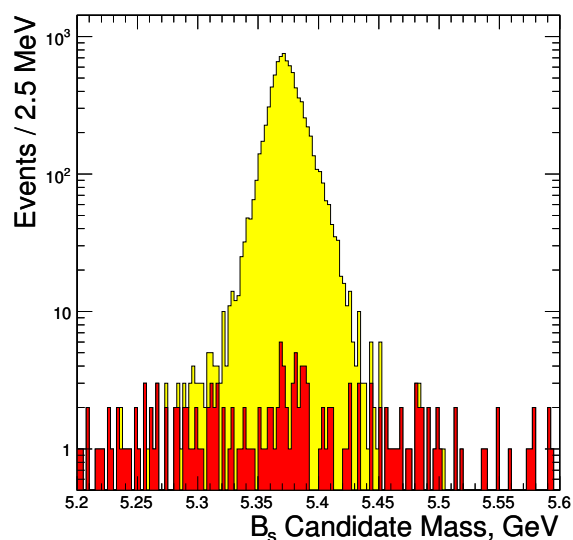
Figure 8.3: Invariant mass distribution of $B_s \rightarrow (J/\psi) \phi$ **after the kinematics fit (yellow area). The bottom (red) area is the residual combinatorial background.**
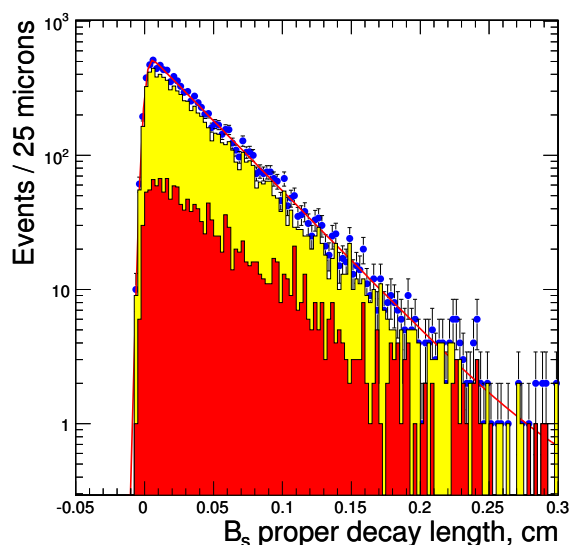
Figure 8.4: Distribution of decay length in the B_s **rest frame showing the** B_s^L **contribution in yellow and the** B_s^H **contribution in red. The red curve is a two - component exponential fit (from ref. [4]).**

observed so far for this decay channel. The resolution on the proper decay length ($c\tau_s$) of the B_s^0 meson is about 30 μm, from which one concludes that the observation of $B_s^0 - \bar{B}_s^0$ oscillations is possible with CMS, provided that the oscillation frequency is close to its present lower limit of 14.4 ps^{-1}.

However, the lifetime difference between the two CP eigenstates B_s^H and B_s^L is too small to be measured directly. Figure 8.4 shows a double exponential fit to the decay length distribution. This task will require an analysis of the angular correlations in the $K^+K^-\mu^+\mu^-$ final state which are different for B_s^H and B_s^L. A corresponding study is in progress. We are investigating in parallel the analogous decay $B_s \rightarrow (J/\psi) \phi$ where $J/\psi \rightarrow e^+e^-$. This decay will increase the B_s^0 sample, but the reconstruction of low-momentum electrons is notoriously difficult.

8.2   Silicon pixel sensors

The pixel detector consists of three concentric cylindrical layers, 53 cm long, with radii of 4.4, 7.3 and 10.2 cm, and forward/backward wheels. The pixel sensors are mounted on segmented silicon plates and are connected by indium bump bonds to the readout chips. The analog signals are read out using charge sharing between pixels to determine the coordinates more accurately. Details can be found in previous annual reports.

We have tested prototypes of sensors (pixel size 125×125 μm^2) with 105 - 225 GeV pions in the H2 beam line of the CERN SPS and measured the charge collection, hit detection efficiencies and the Lorentz angle (6; 7; 8; 9). Oxygenated pixel sensors with p-spray isolation (manufactured by CiS, Erfurt) were chosen. The pixel cell size was finally fixed to 100×150 μm^2.
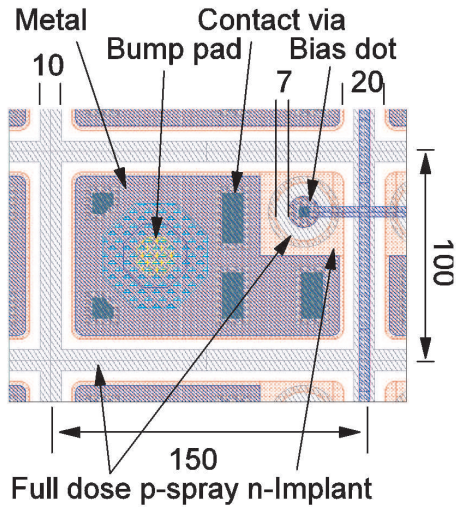
Figure 8.5: Pixel cell layout for the barrel detector.

Figure 8.5 shows a sketch of the final pixel cell layout.

In pixel sensors effects due to irradiation can be investigated with the grazing angle technique (8). As shown in Fig. 8.6 the surface of the sensor is tilted by a small angle (15°) with respect to the pion beam. The charge measured by each pixel along the x direction samples a different depth z in the sensor. The precise entry point is measured with our silicon beam telescope which measures tracks with an r.m.s. position resolution of about 1 μm (10). For un-irradiated sensors the cluster length determines the depth over which charge is collected in the sensor.

The profiles measured with an un-irradiated sensor and with a sensor irradiated to a fluence of 6×10^{14} n_{eq}/cm^2 are shown in Fig. 8.7 as a function of the distance x from the beam entry point. This fluence corresponds to the first four years of LHC operation for the innermost layer. The un-irradiated sensor was operated at a bias voltage of 150 V, well above its depletion voltage of 70 V). The irradiated sensor was operated at bias voltages between 150 V
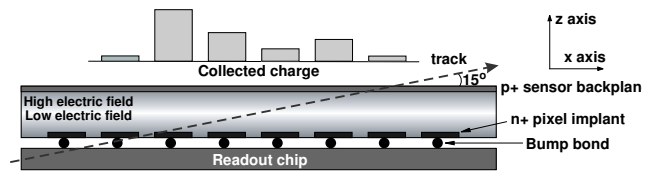

Figure 8.6: Grazing angle method to determine the charge collection profiles.
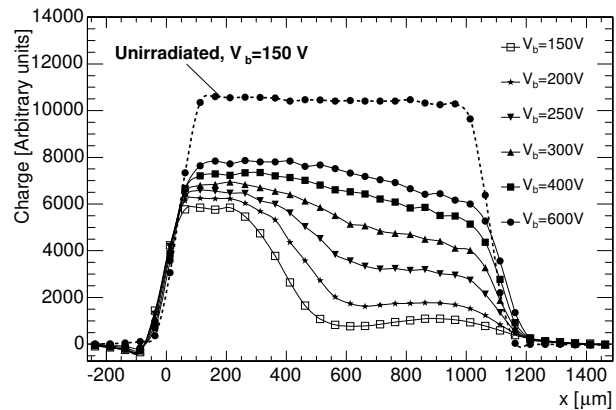

Figure 8.7: Charge collection profiles measured with an un-irradiated (dashed line) sensor and a sensor irradiated to 6×10^{14} n_{eq}/cm^2 (solid lines). The latter is operated at bias voltages V_b between 150 V and 600 V.
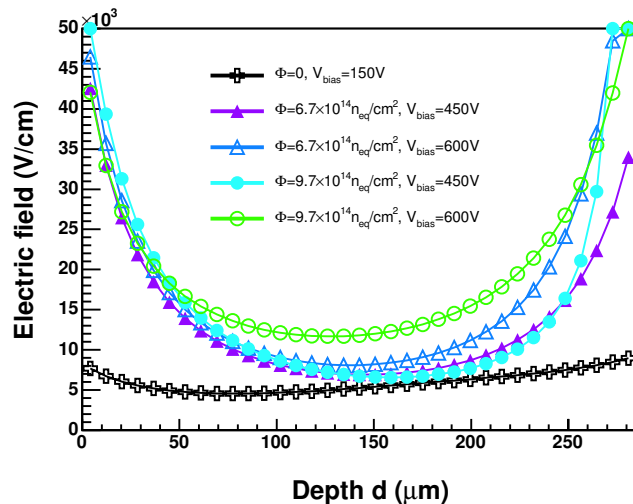

Figure 8.8: Electric field as a function of sensor depth (from ref. [7]). The regions immediately below the surfaces ($\sim 20\mu$m) are affected by large systematic uncertainties (not shown).

and 600 V. It appears to be partly depleted at 150 V, but a second peak is observed at large x. By increasing the bias voltage one also increases the amplitude of the second peak, as more charge is collected from the sensor side close to the backplane, while the increase at the n+ side is about 30%. At 600 V charge collection is saturated but the profile is not uniform due to the trapping of carriers produced far from the collecting electrode.

When a magnetic field is applied along the x-direction, the charge is deflected in the y-direction towards the adjacent pixel row. A measurement of the charge distribution among adjacent pixels yields the Lorentz angle θ_L as a function of x, and hence sensor depth. The Lorentz angle appears to depend on depth. A measurement of θ_L as a function of depth determines the behaviour of the electric field. Using a known empirical parameterization of the mobility one can extract the electric field as a function of sensor depth (7). The electric field reaches maxima below both surfaces and a minimum in the bulk center (Fig. 8.8). This behaviour in irradiated sensors does not correspond to the classical picture of a partially depleted sensor, but can be described by a double junction model (11).

A detailed modeling (PIXELAV) of charge collection in heavily irradiated sensors was developed in collaboration with M. Swartz from Johns Hopkins University. This model takes into account e.g. the charge deposition by hadrons, a 3D intrapixel electric field map, the mobility, diffusion and trapping, and a simulation of the electronic noise (12). Simulations were performed and tuned on the tests results described above for the 125×125 μm^2 sensors. The charge collection profiles for a sensor irradiated to a fluence of 2×10^{14} n$_{eq}$/cm^2 and operated at several bias voltages are presented in Fig. 8.9. The measured profiles are compared to the simulated PIXELAV profiles. The simulation describes the measured charge collection profiles rather well, both in shape and normalization. In particular, the wiggle observed at low bias voltages is also described correctly.

Our simulations can now be applied to the final pixel dimensions of 100×150 μm^2. Since charge is shared among several pixels on can improve on the position resolution by applying the so - called η correction (13). The hit position is first calculated with the center of gravity method. The η fraction is defined as the non - integer part of the reconstructed pixel number. Figure 8.10 shows the distribution of η for all events, where $\eta = 0$ corresponds to the

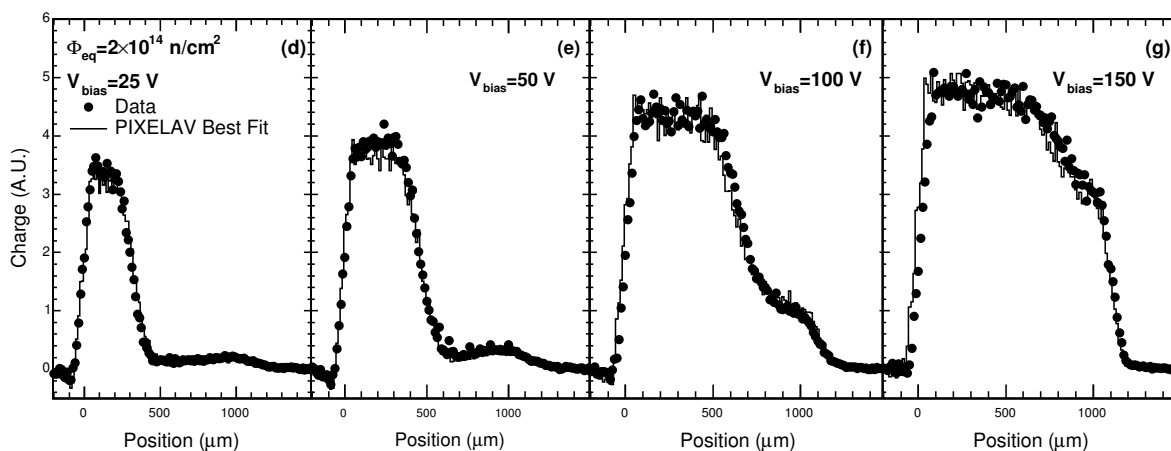**Figure 8.9: Measured (dots) and simulated (histogram) charge collection profiles for a sensor irradiated to a fluence of 2×10^{14} n$_{eq}$/cm^2 and operated at several bias voltages. The simulation was performed with the PIXELAV software (from ref. [11]).**

center of the pixel cell and $\eta = \pm 0.5$ to the borders. The measured distribution is almost flat in the pixel regions close to the pixel borders but has a dip at the center. The peak at $\eta = 0$ is due to single pixel clusters. For each η one then associates a corrected value given by the function

$$F(\eta) = \frac{\int_{-0.5}^{\eta} \frac{dN}{d\eta}\, d\eta}{\int_{-0.5}^{0.5} \frac{dN}{d\eta}\, d\eta} - \frac{1}{2}, \qquad (8.12)$$

where η is in pixel units. The $F(\eta)$ function is shown in Fig. 8.11. The corrected position is calculated by adding $F(\eta)$ to the integer part of the pixel number.

Figure 8.12 shows the residual distribution for clusters of two pixels, simulated for a sensor irradiated to 5.9×10^{14} n$_{\mathrm{eq}}$/cm^2, and for tracks with an incident angle of $20°$ with respect to the normal to the sensor surface. The distribution before correction (left) is not described by a single Gaussian and is affected by large systematic errors which depend on the hit position. Systematic errors can be largely reduced by applying the η-correction (Fig. 8.12, right). This simulation shows that resolutions below 15 μm can be achieved after irradiation. A comparison with beam tests of the final sensors will be performed in 2006.
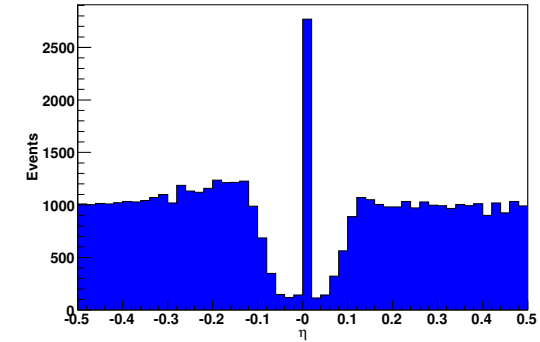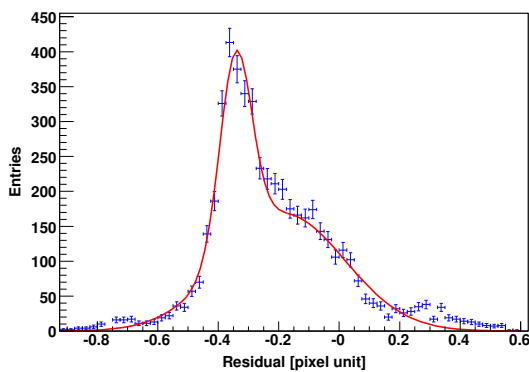

Figure 8.10: Distribution of the reconstructed impact position within a single pixel for perpendicular tracks.
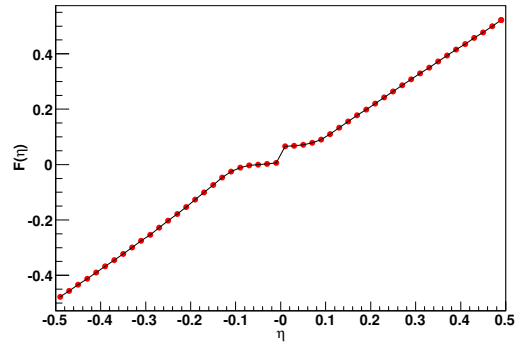

Figure 8.11: Correction function $F(\eta)$ (from ref. [14]).
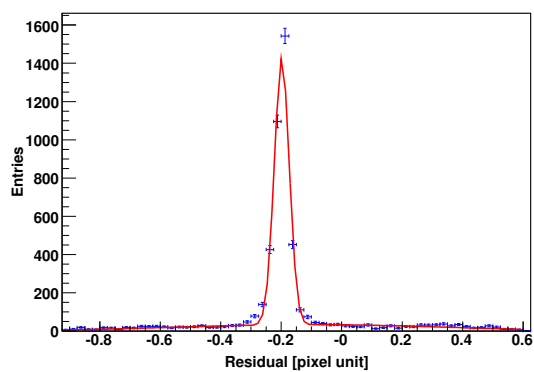

Figure 8.12: Residual (simulated - reconstructed hit) distribution for tracks with an incident angle of $20°$. The distributions are calculated without (left) and with η-corrections (right) and are not corrected for the Lorentz shift due to the magnetic field. The simulated data points are represented by markers and the continuous line is a double-Gaussian fit to the distribution (from ref. [14]).

8.3   Readout electronics

We have also contributed to the readout chip (ROC), the design of which is under the direct responsibility of PSI. The ROC, manufactured in CMOS 0.25 μm technology by IBM, has a much higher yield (80%) than our previous prototype in DMILL radiation hard technology (20%). The first complete module (16 ROC chips, each reading 52×80 pixels) were irradiated with 300 MeV/c pions at PSI (Fig. 8.13 and 8.14). The purpose was to measure the efficiency as a function of inclination ϕ and readout threshold, and to check the timing performance. The incoming intensity was typically 40 MHz/cm^2 (corresponding to the rate in the first pixel layer at 4.4 cm in LHC). The trigger was provided by two scintillators of dimensions $2 \times 2 \times 2$ mm^3 (which counted at a rate of 1 MHz) in coincidence with an americium radioactive source to simulate the level 1 trigger in CMS. The data analysis is in progress (15).
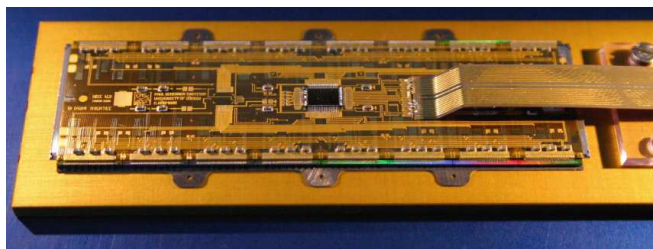

Figure 8.13:   First assembled module consisting of 16 PSI46V2 readout chips bump-bonded to a sensor with 66'560 pixels.
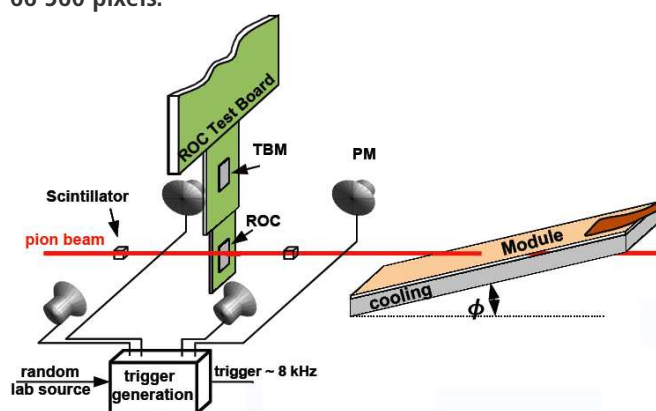

Figure 8.14: Setup for the beam tests at PSI.

8.4   Mechanical support structure

The Institute's workshop is building the support structure for the barrel pixel detector and the service tubes along the beam line.   The pixel detector consists of three 57 cm long layers (Fig. 8.15) equipped with silicon pixel modules and two 2.2 m long service tubes.   Two vertically separated half shells will be introduced into the CMS detector. The support structure consists of individual ladders built of pure aluminum tubes with trapezoidal cross sections and wall thickness of 300 μm.
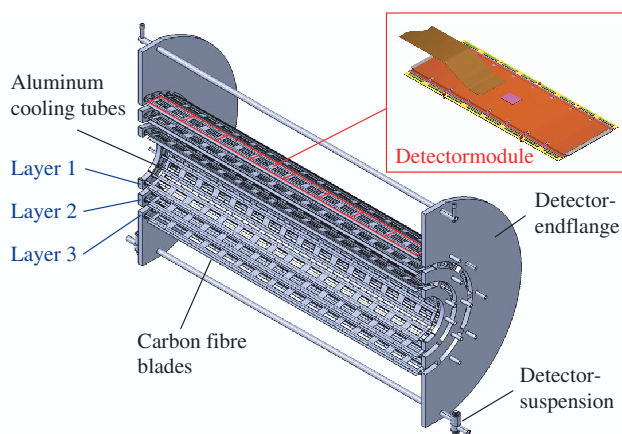

Figure 8.15:   Half shell of the support structure with the three detector layers.

Custom made 240 μm thick carbon fiber blades which support the pixel modules are glued to the tubes, forming the detector segments (Fig. 8.16). Four to five of these tubes are then laser welded to an aluminum container which distributes the coolant. The manifold provides the cooling of the detector modules to about -10°C with C_6F_{14}. Support frames on both ends
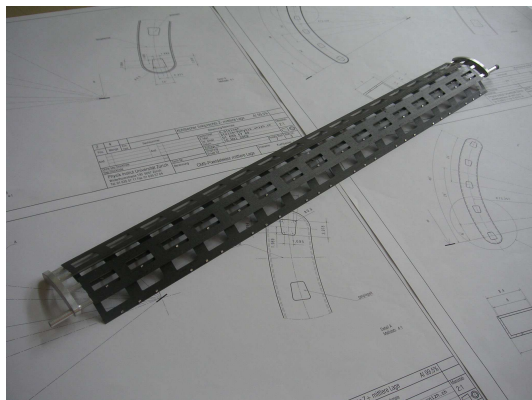
Figure 8.16: Prototype segment. The aluminum tubes are laser welded to the end-flange containers that distribute the cooling fluid.
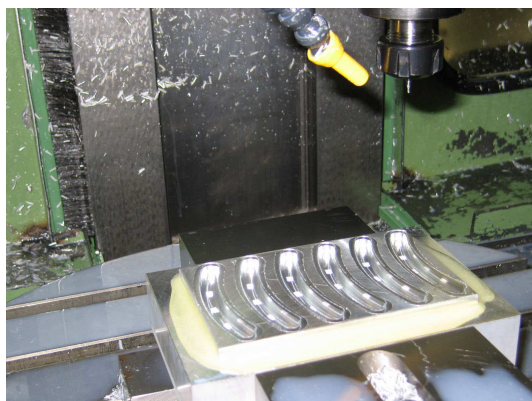

Figure 8.17: Production of the carbon fiber blades (upper picture) and of the cooling containers (lower picture) on the milling machines of the Physik - Institut.

connect the segments and form a detector layer half shell. The flanges consist of thin fiberglass frames (FR4) filled with foam (Airex) covered by carbon fiber blades. This technique guarantees stability and precision for a minimum mass. Mass production of the various components (blades, cooling containers, etc.) is performed in our workshop (Fig. 8.17). The laser welding technique (in collaboration with industry) was strongly improved. We have upgraded the welding equipment to prevent leakage of the coolant and have obtained higher quality welding seams than achieved before.

The electrical power, control and optical signals and the coolant are transferred to the detector through supply tubes. The forward and backward supply tubes are mechanically connected and carry the pixel detector. The structure is made of tubes and is filled with foam. The motherboards (Fig. 8.18) holding the optical hybrids for analog and digital controls, will be installed near the detector. The outer ends contain power regulators and connectors for the electrical and optical lines, and the central region the digital control boards and slow controls, such as voltages, currents, temperatures, pressures and humidity.

The project proceeds according to schedule. The 800 modules required for the three pixel layers will be assembled at PSI. In 2006 our group will perform further beam tests at CERN. Production of the parts for the three layers is proceeding in our workshop. Prototypes of the service tubes will be built in 2006. The pixel detector will be introduced into CMS after the LHC commissioning in 2007, to prevent damage during initial beam tuning. We are preparing a test support structure for the 2007 pilot run, consisting of a half shell partially equipped with detectors.
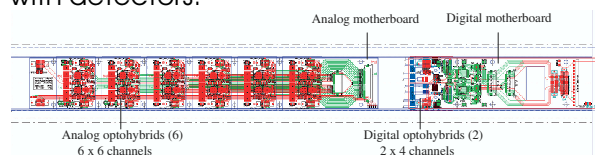

Figure 8.18: Sketch of the readout slot with the analog and digital motherboards holding the optical hybrids.

[1] E. Alagöz *et al.*, CMS TDR I : Software and detector performance, CMS - TDR - 08, CERN-LHCC-2006-001.

[2] S. Eidelman *et al.* (Particle Data Group), Phys. Lett. **B 592** (2004) 1.

[3] A.S. Dighe *et al.*, Phys. Lett. **B 269** (1996) 144; Eur. J. Phys. **C6** (1999) 647.

[4] K. Prokofiev, PhD Thesis, Universität Zürich (2005); K. Prokofiev Proc. 10th Int. Conf. on B-Physics at Hadron Machines (BEAUTY 2005), Assisi, Nucl. Phys. **B** Proc. Suppl. **156** (2006) 109.

[5] T. Speer *et al.*, Proc. of the Workshop on Tracking in High Multiplicity Environments (TIME 2005), Zurich (in print); T. Speer and R. Frühwirth, Comp. Phys. Comm (in print).

[6] R. Kaufmann, PhD Thesis, Universität Zürich (2001).

[7] A. Dorokhov, PhD Thesis, Universität Zürich (2005); A. Dorokhov *et al.*, Proc. Vertex 2004 Conf., Como, 2004, Nucl. Instr. Meth. in Phys. Research **A** (in print), prep. physics/0412036.

[8] A. Dorokhov *et al.*, Nucl. Instr. and Meth. in Phys. Research **A 530** (2004) 71.

[9] T. Rohe *et al.*, Nucl. Instr. and Meth. in Phys. Research **A 552** (2005) 232.

[10] C. Amsler *et al.*, Nucl. Instr. and Meth. in Phys. Research **A 480** (2002) 501.

[11] V. Chiochia *et al.*, Proc. 2004 IEEE Trans. on Nucl. Sc. **52** (2004) 1067; V. Chiochia *et al.*, Proc. 10th Eur. Symp. on Semiconductor Detectors, Wildbad-Kreuth, Nucl. Instr. Meth. in Phys. Research **A** (in print), prep. physics/0506228.

[12] M. Swartz, Nucl. Instr. and Meth. in Phys. Research **A 511** (2003) 88.

[13] E. Belau *et al.*, Nucl. Instr. and Meth. **214** (1983) 253.

[14] E. Alagöz, V. Chiochia, M. Swartz, Proc. of the Workshop on Tracking in High Multiplicity Environments (TIME 2005), Zurich, Nucl. Instr. Meth. in Phys. Research **A** (in print), prep. physics/0512027.

[15] C. Hörmann, PhD Thesis, Universität Zürich, in preparation.